Quantitative Study of Fracture by Acoustic Emission From Cracks

KWANG YUL KIM, WOLFGANG SACHSE and PAONAN HSIEH†

Department of Theoretical and Applied Mechanics, Cornell University, Ithaca, New York – 14853 USA

ABSTRACT

In quantitative acoustic emission (AE) studies of fracture, transient elastic waves accompanying the formation of point-like small cracks are analyzed to recover the spatial and temporal characteristics of fracture processes. This paper summarizes our studies of Mode I cracks generated by indentation and thermal cooling in a brittle material such as glass, and Mode I and mixed mode cracks formed under tensile loading of a 7075-T6 aluminum compact tension (CT) specimen.

Included in our investigation are determination of location of a generated crack, its orientation and AE radiation pattern, the time-dependent crack velocity, and identification of the fracture mode in addition to determination of the critical rupture stress, the critical crack tip opening displacement *(CTOD)*, and the effective microstructural gauge length of a Mode I crack, provided that the Mode I stress intensity factor is known.

† Present Address: Battelle Memorial Institute, Columbus, OH - 43201

KEYWORDS

Fracture; crack; acoustic emission; moment tensor; radiation pattern; dipole strength; source-time function; Dugdale-Barenblatt model; crack velocity; critical rupture stress; crack tip opening displacement; microstructural gauge length.

INTRODUCTION

Successful inplementation of acoustic emission (AE) techniques used for *in situ* structural integrity monitoring applications depends on accurate indentification and characterization of an AE source such as the formation of a crack. Transient elastic waves accompanying the formation of a crack propagate through the medium and in the bounded structure reflect and refract at the surface, thereby providing a convenient means for detection of AE signals and monitoring. The propagation of transient elastic waves in the bounded medium was investigated in detail by various authors (Knopoff, 1958; Hsu *et al.*, 1977; Ceranoglu and Pao, 1981) and their results are utilized to remove the effects

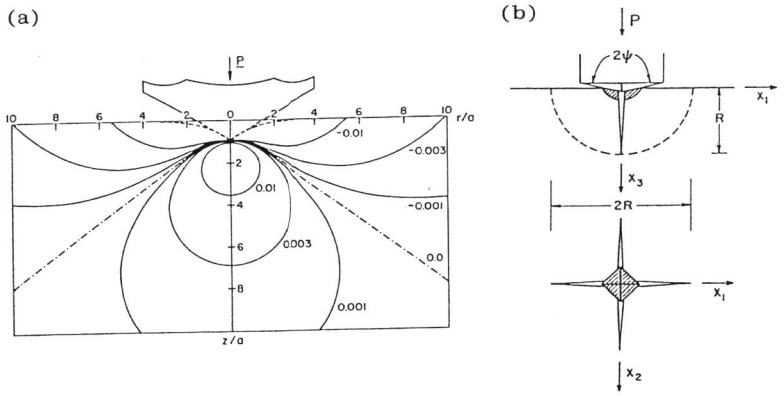

Fig. 1. Indentation crack. (a) Contours of hoop stresses generated by a conical indenter; (b) Side view and top view of the Vickers indentation crack.

of the structure from the detected AE signals through the use of the appropriate signal processing techniques, so as to elicit the characteristics of the AE source. An AE source associated with the formation of a crack is conveniently represented by a *moment tensor* (Aki and Richards, 1980; Doornbos, 1981; Kim and Sachse, 1986b, c) whose spatial and temporal characteristics contain valuable information about the fracture processes and its dynamics (Kim and Sachse, 1986c, 1988). In this paper we describe the AE moment tensor obtained from analysis of detected AE signals in terms of various parameters used in fracture mechanics and summarize our recent progress made towards achieving this goal.

EXPERIMENT

In our experiments emphasis has been given to generating small microcracks which can be well approximated as point sources of acoustic emission. Reproducible microcracks of Mode I type were generated on/near the surface of a specimen of soda-lime glass by employing an indentation technique or a thermal cooling of a small scratch on the surface of the specimen. Microcracks generated in a compact tension (CT) specimen of 7075-T6 aluminum were unpredictable and uncontrollable in terms of their location, fracture mode and orientation. At least four AE sensors are needed to locate an AE source but in most experiments described here, nine broadband sensors were used to detect the AE signals. Indentation cracks of Mode I type were generated by pressing both a conical indenter and a Vickers indenter squarely onto the surface of the glass plate. Indentation of the conical indenter resulted in formation of a penny-shaped crack lying normal to the surface and resembling the contours of a tensile hoop stresses generated beneath the indenter, which is shown in Fig. 1(a), where P is a load applied to the indenter, the axes r and z of the polar cylindrical coordinate system (r, θ, z) are normalized

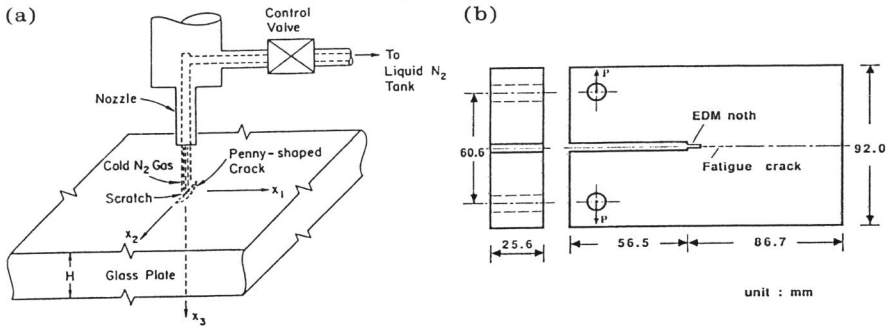

Fig. 2. (a) Thermal crack generation setup; (b) Aluminum CT specimen.

against a contact radius a and values shown around the contours of the hoop stress are also normalized with respect to the contact pressure $P/\pi a^2$. The specific angular orientation of the crack, θ_c, was rather arbitrary because of a circular symmetry of the indenter and depends on such factors as local inhomogeneity and geometry of the indenter tip. The Vickers indenter produced two mutually perpendicular cracks of a half-penny shape oriented normal to the surface along the indenter diagonals, as shown in Fig. 1(b). Other cracks of Mode I type were also generated by blowing cold nitrogen gas derived from a liquid nitrogen tank through a fine nozzle onto the tiny scratch made with a diamond scribe on the surface of the specimen. The generated cracks were observed again lying normal to the surface along the scratched direction and resembled an almost cut-out, sectioned penny (see Fig. 2(a)). The CT aluminum specimen shown in Fig. 2(b) was notched by an electron discharge machine (EDM) and subsequently fatigued to sharpen the crack tip front and then loaded in a tensile testing machine for generation of microcracks ahead of the fatigue crack.

For detection of Mode I cracks generated in a glass plate with thickness H, one AE sensor was situated at the epicenter and several other sensors were located at various angular positions on the circle of radius $2H$ centered at the epicenter on the side opposite from the AE source. Usually capacitive displacement transducers were used but for determination of the AE radiation pattern eight small piezoelectric transducers of 1.3 mm^2 active area were employed at the off-epicental positions. For the aluminum CT specimen, eight piezoelectric sensors were located at points ahead of the fatigue crack front, on the specimen faces normal to the fatigue crack front and parallel to a loading direction.

The capacitive displacement transducers were connected to charge amplifiers whose bandwidth extended from 10 kHz to 10 MHz. The outputs of the piezoelectric transducers were amplified by preamplifiers with bandwidth of 10 kHz to 2 MHz. The outputs of all these amplifiers were connected to transient digitizers which recorded them at a 30 or 60 MHz sampling rate and with 10-bit resolution. The recorded data were visualized

on a x-y display and brought into the microcomputer for subsequent data analysis and storage.

THEORY

Moment Tensor Representation of an AE Source

It was previously mentioned that AE dipole sources including the formation of a crack, dilatation, some phase transformations were conveniently represented by the moment tensor $\mathbf{M}$. If the excitation body force $f(\xi,t)$ acts at location ξ in a small volume $\Delta V(\xi)$ which can be replaced by a point source about ξ^0, then the element of the moment tensor is given by

$$M_{jk}(\xi^0,t) \;=\; \int_V f_j(\xi,t)\;\Delta\xi_k\;dV(\xi) \tag{1}$$

where t denotes time and $\Delta\xi_k = \xi_k - \xi_k^0$. Making use of the Green's function G_{ji} (Aki and Richards, 1980), the displacement $\mathbf{u}^{(d)}(\mathbf{x},t)$ at location $\mathbf{x}$, due to an AE dipole source $\mathbf{M}$, is expressed by

$$u_i^{(d)}(\mathbf{x},t) \;=\; M_{jk}(\xi^0,t) * G_{ji,k}(\mathbf{x},\xi^0;t) \quad (i,j,k=1,2,3) \tag{2}$$

where the symbol $*$ denotes a convolution integral in time and $G_{ji,k}$ ($\equiv \partial G_{ji}/\partial\xi_k$) is the *dipole Green's function*. In the above equation and those following the summation over repeated indices is implied unless othewise specified.

Using the equation of force equilibrium, (1) can be written as

$$M_{jk} \;=\; \int_V \Delta\sigma_{jk}\;dV(\xi) \tag{3}$$

where $\Delta\sigma_{jk}$ denotes a component of the *glut stress* resulted in the source volume.

Eqs. (1), (2) and (3) are general, that is, they can be used to describe an AE source whether it be subjected to elastic or plastic deformations. When the source region undergoes a purely elastic deformation, (3) becomes

$$M_{ij} \;=\; \int_V c_{ijkl}\Delta\epsilon_{kl}\;dV(\xi) \;=\; \int_A c_{ijkl}\;[u_k]\;\hat{n}_l\;dA \tag{4}$$

where c_{ijkl} is the *Hookean stiffness tensor*, and

$$\Delta\epsilon_{kl} \;\equiv\; \{[u_k]_{,l} \;+\; [u_l]_{,k}\}\,/2 \tag{5}$$

is a component of the *glut strain*, and $[u_k]$ denotes the displacement discontinuity in the k-th direction on the source surface element dA whose outward normal is represented by a unit vector $\hat{\mathbf{n}}$. For a point source for which $\Delta\sigma_{ij}$ or $[u_k]$ can be treated as constant, the moment tensor is simply

$$M_{ij} \;=\; \Delta\sigma_{ij}\cdot\Delta V \tag{6}$$

$$\;=\; c_{ijkl}\Delta\epsilon_{kl}\;\Delta V \;=\; c_{ijkl}\;[u_k]\;\hat{n}_l\;\Delta A \quad \text{(elastic)} \tag{7}$$

$\Delta\sigma_{ij}$ and $c_{ijkl}[u_k]\hat{n}_l$ are sometimes called the *volume* and *surface moment density tensor*, respectively.

In a purely elastic case, M_{ij} in (7) can be diagonalized by a proper rotation of the coordinate system to find the angle θ between the displacement jump $[\mathbf{u}]$ and the crack normal $\hat{\mathbf{n}}$. If the coordinate system is chosen such that the diagonal elements of the diagonalized moment tensor $\mathbf{M}'$ have the relation $M_1' \geq M_2' \geq M_3'$, (Hsieh, 1987), then it can be shown that

$$\tan^2\left(\frac{\theta}{2}\right) \;=\; \frac{M_1' - M_2'}{M_1' - M_3'} \tag{8}$$

and the AE source volume ΔV is given by

$$\Delta V \;\equiv\; |\mathbf{u}\cdot A\hat{\mathbf{n}}| \;=\; M_2'/\lambda \tag{9}$$

where λ is the *Lamè* constant of the material.

Mode I Crack AE Source and AE Radiation Pattern

If one of the orthogonal coordinate axes, say the x_1-axis, coincides with the normal to the crack plane of a Mode I crack for whcih the shear stress contribution vanishes, then according to (3) M_{ij} can be written as

$$M_{ij}(t) \;=\; M_{ij}\;\delta_{ij}(t) \quad \text{(no summation implied)} \tag{10}$$

where δ is a Kronecker delta. The time function associated with crack formation is primarily governed by the crack velocity. The assumption is made that all the elements of the moment tensor associated with the same crack share the same time function denoted by $S(t)$, which is generally known to be like a ramp-step with a particular ramp risetime Δ. Normalizing $S(t)$ and denoting it by $\hat{S}^{(d)}(t)$, which has unit amplitude when $t \gg \Delta$, then M_{ij} in (10) can be written as

$$M_{ij}(t) \;=\; D_{ij}\;\hat{S}^{(d)}(t)\;\delta_{ij} \quad \text{(no summation implied)} \tag{11}$$

where D_{ij} is known as the *dipole strength*.

Most of the two mutually perpendicular, half-penny shaped cracks created by Vickers indentation are exposed to the free surface of the specimen for which $\sigma_{33} = 0$ and so, $M_{33} \simeq 0$. In our experiments, these cracks were also observed to be almost identical both in shape and in size and therefore, $D_{11} \simeq D \simeq D_{22}$. The moment tensor associated with the Vicker cracks can then be expressed as

$$\mathbf{M} \;=\; D\begin{bmatrix} 1 & 0 & 0 \\ 0 & 1 & 0 \\ 0 & 0 & 0 \end{bmatrix}\hat{S}^{(d)}(t), \tag{12}$$

$$\text{and}\quad u_3^{(d)}(\mathbf{x},t) \;=\; D\;\hat{S}^{(d)}(t) * \left[G_{13,1}(\mathbf{x},\xi^0;t) \;+\; G_{23,2}(\mathbf{x},\xi^0;t)\right]$$

$$\;=\; D\;\hat{S}^{(d)}(t) * G^{(d)}(\mathbf{x},\xi^0;t) \tag{13}$$

$$\text{where}\quad G^{(d)}(\mathbf{x},\xi^0;t) \;\equiv\; G_{13,1}(\mathbf{x},\xi^0;t) \;+\; G_{23,2}(\mathbf{x},\xi^0;t). \tag{14}$$

$G^{(d)}(\mathbf{x}, \xi^0; t)$ can be calculated at epicentral and off-epicentral receiver positions using the algorithm developed by Ceranoglu and Pao (1981).

Let the polar cylindrical angular coordinate θ be measured relative to the x_1-axis which is chosen to be parallel to the crack normal whose angle is specified by θ_c, for either the indentation cracks generated by the conical indenter or for the thermal cracks. Then the displacement $u_3^{(d)}(\mathbf{x}, t)$ in (2) detected at the receiver location with angular coordinate θ, equidistant from the AE source, exhibits the following radiation pattern (Kim and Sachse, 1986a)

$$u_3^{(d)}(\theta, t) = a(t)\ [b(t) + cos^2(\theta - \theta_c)]. \tag{15}$$

The radiation constant b(t) determined from the P-ray arrival can be expressed in terms of moment tensor component D_{ii} (i = 1, 2, 3; no summation is implied) and has been used to determine each D_{ii} (Kim and Sachse, 1986b, c).

The procedures and methods of determining the moment tensor M_{ij}, its magnitude D_{ij} and AE radiation pattern for a Mode I crack were described in detail previously (Kim and Sachse, 1986a, b, c). As can be seen in (2), the normalized AE source-time function $\hat{S}^{(d)}(t)$ can be recovered by deconvolving the measured displacement signal $u_3^{(d)}(\mathbf{x}, t)$ with the pertinent, calculated Green's function and by normalizing the resulting time function.

Relationship between Indentation Fracture Mechanics and a Dipole AE Source

In this subsection we will describe the indentation fracture and its dynamics in terms of the dipole strength and dipole time function. Vickers indentation cracks have been chosen for this purpose because the orientation, shape and size of these cracks were clearly defined and could be easily measured with an optical microscope.

Based on a dimensional analysis Lawn and Fuller (1975) derived a very simple expression for the Mode I stress intensity factor, K_{Ic}, applied to an indentation crack

$$K_{Ic} = \frac{1}{\pi^{3/2} \tan\psi}\left(\frac{P}{R^{3/2}}\right) = 7.256 \times 10^{-2}\left(\frac{P}{R^{3/2}}\right) \tag{16}$$

where P is the load applied to the indenter, ψ is the half-angle (68°) between the Vickers indenter faces and R is the radius of the resulting half-penny crack. The crack extension force G_c is given by

$$G_c = K_{Ic}^2(1 - \nu^2)/E \tag{17}$$

where ν and E are the Poisson's ratio and Young's modulus of a specimen, respectively. They are 0.217 and 73.03 GPa for soda-lime glass. Next we apply the Dugdale-Barenblatt model (Dugdale, 1960; Barenblatt, 1962) for the calculation of G_c. Referring to Fig. 3, it is seen that for brittle solids

$$G_c = \sigma_c u_c/2 = \sigma_c \ell \epsilon_c/2 = 2\gamma \tag{18}$$

where σ_c, u_c, ℓ, ϵ_c and γ are the *critical rupture stress, crack tip opening displacement (CTOD), microstructural gauge length* involved in the rupture process, the *critical cut-off*

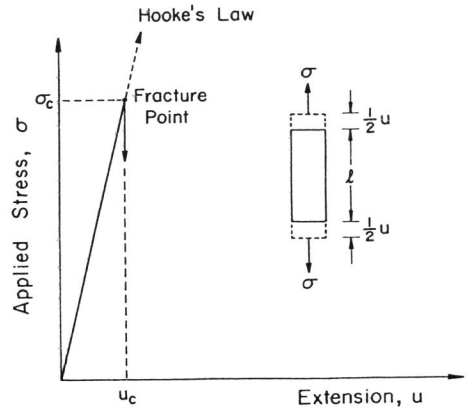

Fig. 3. An idealized stress-extension curve for a perfectly brittle solid.

strain, and the *surface energy of the crack plane*, respectively. For a crack in a brittle solid, the following relation holds at the crack tip

$$\epsilon_c = \sigma_c/E = u_c/\ell \tag{19}$$

If the area swept by the crack front of radius r is denoted by $A(t)$ whose final size A_f is equal to $\pi R^2/2$, the area of the half-penny crack and the dipole function $D\hat{S}^{(d)}(t)$ in (12) can be expressed as

$$D\hat{S}^{(d)}(t) = \sigma_c A(t)\ell = (1/2)\pi\sigma_c\ell\, r^2(t) \tag{20}$$

Remembering that when $t \gg \Delta$ (risetime), $\hat{S}^{(d)}(t) = 1$ and $A(t) = A_f$, one obtains

$$D = \sigma_c A_f \ell = E A_f u_c \tag{21}$$

$$\sigma_c = E\epsilon_c = 2EG_c A_f/D. \tag{22}$$

Combining (17), (18), and (21), one finds a relationship between the applied load P and the dipole stregth D.

$$\frac{P^2}{R} = \frac{\pi^2 \tan^2\psi}{1 - \nu^2}\,\sigma_c D = 63.45\ \sigma_c D. \tag{23}$$

This equation predicts that a plot of (P^2/R) versus D will be a straight line whose slope is 63.45 σ_c. The linear crack velocity v_c can be obtained by differentiating (20) with respect to time, with the result

$$v_c \equiv \frac{dr}{dt} = \frac{A_f}{\pi r}\,\frac{d\hat{S}^{(d)}(t)}{dt}. \tag{24}$$

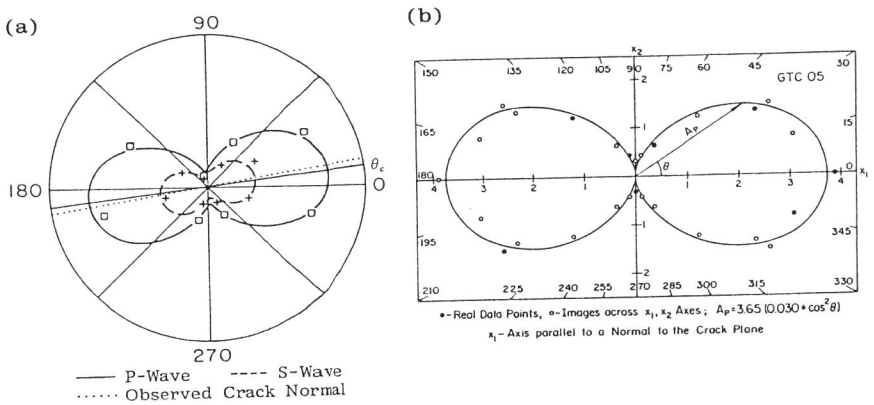

Fig. 4. (a) P- and S-wave radiation patterns of a conical indentation crack; (b) P-wave radiation pattern of a thermal crack.

DATA ANALYSIS AND RESULTS

The radiation patterns of Mode I cracks generated by a conical indenter in a glass plate were obtained by fitting the first arrival P- (longitudinal) and S- (shear) wave amplitudes measured at eight different receiver positions to (15) by the nonlinear squares method to determine a, the radiation pattern constant b, and θ_c, the angular coordinate of the crack normal. A typical radiation pattern obtained from these constants is shown in Fig. 4(a) where the calculated crack normal is in very good agreement with that observed with an optical microscope, indicated by a dotted straight line. We note that the radiation patterns of both the P- and the S- wave arrivals exhibit a very similar result, both being aligned in the same direction as expected from (15), and implying that either can be used to determine the orientation of a Mode I crack. In a similar way, the P-wave radiation pattern of the signals emitted by a thermal crack whose normal is empirically known to be perpendicular to the scratch and also to be parallel to the surface is shown in Fig. 4(b) by taking θ_c to be zero. The value of b indicated in the figure is found to be close to zero.

Fig. 5 shows the load applied to the Vickers indenter versus $R^{3/2}$, where R is the radius of the resulting half-penny shaped crack formed. A least squares fit of the data into (16) yields a staight line whose slope is found to be 324 N/mm$^{3/2}$ from which one obtains from (16), (17) and (18)

$$K_{Ic} = 0.744 \text{ MN/m}^{3/2}, \quad G_c = 7.23 \text{ J/m}^2, \quad \gamma = 3.62 \text{ J/m}^2. \tag{25}$$

The fracture surface energy γ listed above for soda-lime glass compares very well with the result obtained by Wiederhorn (1969) of 3.91 J/m^2, which was obtained by using a double-cantilever beam specimen.

The dipole strength D in (12) was determined from the displacement signals detected

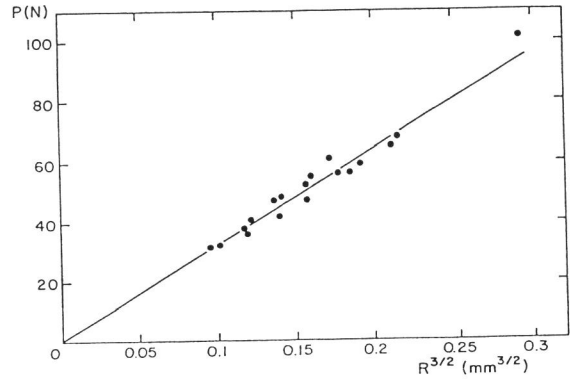

Fig. 5. Applied load P vs. $R^{3/2}$; R: Crack radius.

by three off-epicentral capacitive transducers located on the $2H$ radius circle centered at epicenter and situated at 0°, 45°, and 90° from one of the crack normals. A plot of P^2/R versus D is shown in Fig. 6 using (23). The slope of a straight line determined from the least squares fit is 567.4 GPa from which the critical rupture stress is found to be

$$\sigma_c = 8.94 \text{ GPa}. \tag{26}$$

The corresponding critical cut-off strain ϵ_c, the crack tip openning displacement u_c and the microstructural gauge length ℓ can be found from (19), (21) and (22). The results are

$$\epsilon_c = 0.122, \quad u_c = 1.62 \text{ nm}, \quad \ell = 13.2 \text{ nm}. \tag{27}$$

It is seen that the length of the nonlinear cohesive zone, ℓ, is about 80 times longer than the nearest interatomic spacing 0.16 nm between silicon and oxygen atoms.

The dipole source-time function $\hat{S}^{(d)}(t)$ associated with a Vickers crack was obtained by using a deconvolution technique such as the least squares double-iterative scheme (Michaels and Pao, 1985) and is shown in Fig. 7(a). It resembles a parabolic ramp-step function with risetime of about 0.5 μsec. The crack velocity obtained according to (24) is displayed in Fig. 7(b) as a function of the crack front radius. It is seen that a maximum velocity of 1760 m/sec is reached when the crack front radius is at 0.175 mm or about midway towards the final crack size of 0.355 mm. The time taken to reach the final crack size was 0.643 μsec, from which one determines an average crack velocity of 522 m/sec. It should be mentioned, however, that the source-time function shown in Fig. 7(a) is probably more slowing varying than the actual source-time function because of the effects of the finite aperture of the receiving transducers and the bandwidth limitation of the measurement system, which have not been corrected for in the determination of the above source-time function. Consequently, the crack velocity shown in Fig. 7(b) should be understood to be an underestimation of the actual velocity.

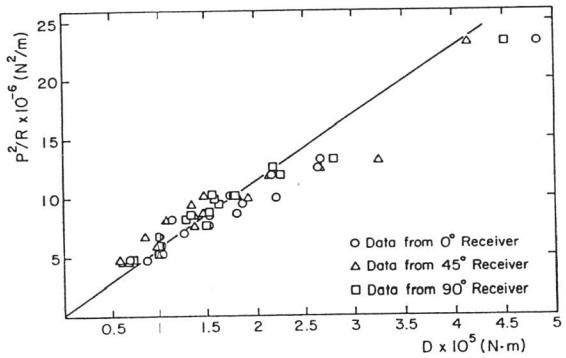

Fig. 6. Plot of P^2/R vs. D ; D: Dipole strength.

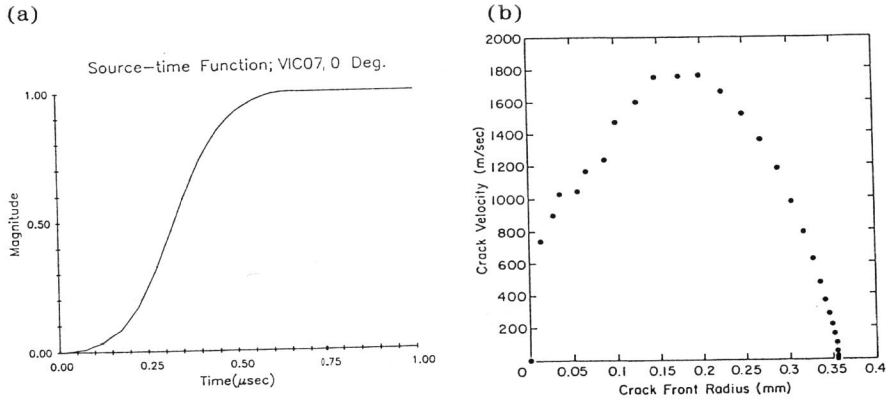

Fig. 7. (a) Unit magnitude source-time function $\hat{S}^{(d)}(t)$ of a Vickers indentation crack; (b) Crack velocity as a function of crack front radius.

The location of AE sources from the microcracks generated ahead of the crack front during tensile loading of the CT aluminum specimen after it was fatigued, was carried out and is shown in Fig. 8. The crack front obtained after the fatigue loading is indicated by the curved solid line in the xy-plane. In the figure the locations of the generated microcracks are indicated by the intersections of the two cross bars. It is seen that they lie near the plane of the crack. Although plastic deformation precedes the formation of the microcracks in the crack tip region, the analysis for finding the angle between the displacement jump $[\mathbf{u}]$ and the crack normal $\hat{\mathbf{n}}$, was performed with (8) in which only elastic deformations are considered. The calculated angles are those between the two crossed bars in these figures. When the two cross bars nearly coincide (i.e. $\theta \approx 0°$), the generated crack is almost of Mode I type. Most of the cracks shown in the figures are seen to be of mixed mode type.

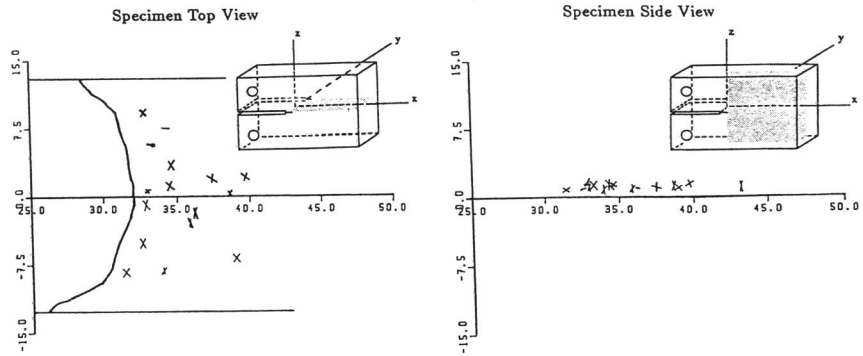

Fig. 8. Calculated source location and crack orientation in a CT aluminum specimen. Directions of two cross bars are those of $[\mathbf{u}]$ and $\hat{\mathbf{n}}$ and are projected onto the xy-plane (left) and the xz-plane (right).

DISCUSSION AND CONCLUSIONS

We have demonstrated that the quantitive AE source characterization method is a very powerful tool for investigation of the fracture and fracture dynamics in britttle solids. Connection between various parameters of fracture and an AE source has been clearly established, enabling us to determine such important parameters as the critical rupture stress and strain, the *CTOD*, the microstructural gauge length, and time-dependent crack velocity. An extension of the work described here can be made to other brittle materials such as ionic, ceramic or semiconducting materials. For single crystals, the crystallographic orientation dependence of fracture can also be investigated. The AE radiation pattern can be used to determine the crack orientation of a pure mode crack. For an accurate determination of the crack velocity, a small aperture, sensitive displacement transducer needs to be developed so that the aperture effect is minimized and the recovered time function of the AE source can be accurately determined.

However, for ductile materials, the relation between an AE source and ductile fracture is complicated because of the plastic deformations in the tip region preceding the formation of the crack. Also, most of the fracture energy spent in the formation of a crack is stored in the material as a result of the irreversible plastic deformation and only a tiny fraction of this energy is released as acoustic emission signals during fracture. Starting with the general formulæ(2) and (3), it is necessary at first to establish a constitutive relation between the glut stress and strain (or displacement discontinuity, $[\mathbf{u}]$) for description of the plastic deformation in the crack tip region and secondly to clearly identify a mechanism of energy release during fracture which results in an acoustic emission. If only the elastic part of fracture energy consumed for crack formation is responsible for the acoustic emission, relations similar to (21) and (22) may hold, albeit in this case predictably much reduced amplitude AE signals result as compared to those arising in

brittle materials. Additional work is required to clarify these points before the AE source characterization method can be unambigously applied for investigation of the ductile fracture in solids.

ACKNOWLEDGEMENTS

The initial portions of this work were sponsored by the National Science Foundation (Solid and Geo-Mechanics Program) under grant MSM-8405466. This work is currently supported by the National Science Foundation through a grant to the Materials Science Center at Cornell University.

REFERENCES

Aki, K. and P. G. Richards (1980). *Quantitative Seismology: Theory and Methods.* Vol. I, Freeman, San Francisco. Chapter 3.

Barenblatt, G. I. (1962). The mathematical theory of equilibrium cracks in brittle solids. *Adv. Appl. Mech.*, **7**, 55-129.

Ceranoglu, A. N. and Y. H. Pao (1981). Propagation of elastic pulses and acoustic emission in a plate. *J. Appl. Mech.*, **48**, 125-147.

Doornbos, D. J. (1981). Seismic moment tensors. In: *Identification of Seismic Sources - Earthquake or Underground Explosions* (E.S. Husebye and S. Mykkeltvert, Eds.), pp. 207-232.

Dugdale, D. S. (1960). Yielding of steel sheets containing slits. *J. Mech. Phys. Solids*, **8**, 100-104.

Hsieh, P. (1987). *Quantitative acoustic emission source characterization in an aluminum specimen.* Ph. D. thesis, Cornell University, Ithaca, New York.

Hsu, N. N., J. A. Simmons and S. C. Hardy (1977). An approach to acoustic emission signal analysis - theory and experiment. *Mater. Eval.*, **35**(10), 100-106.

Kim, K. Y. and W. Sachse (1986a). Acoustic emissions from penny-shaped cracks in glass. I. Radiation pattern and crack orientation. *J. Appl. Phys.*, **59**, 2704-2710.

Kim, K. Y. and W. Sachse (1986b). Acoustic emissions from penny-shaped cracks in glass. II. Moment tensor and source-time function. *J. Appl. Phys.*, **59**, 2711-2715.

Kim, K. Y. and W. Sachse (1986c). Characteristics of an acoustic emission source from a thermal crack in glass. *Intern. J. Fract.*, **31**, 211-231.

Kim, K. Y. and W. Sachse (1988). Study of indentation fracture of brittle solids by acoustic emission. Materials Science Center Report #6523, Cornell University, Ithaca, NY (August 1988). Submitted to *J. Appl. Phys.*

Knopoff, L. (1958). Surface motions of a thick plate. *J. Appl. Phys.*, **29**, 661-670.

Lawn, B. R. and E. R. Fuller (1975). Equilibrium penny-like cracks in indentation fracture. *J. Mater. Sci.*, **10**, 2016-2024.

Michaels, J. E. and Y. H. Pao (1985). The inverse source problem for an oblique force on an elastic plate. *J. Acoust. Soc. Am.*, **77**, 2005-2011.

Wiederhorn, S. M. (1969). Fracture surface energy. *J. Am. Ceramic Soc.*, **52**, 99-105.